Eukaryotic class 1 translation termination factor eRF1 – the NMR structure and dynamics of the middle domain involved in triggering ribosome-dependent peptidyl-tRNA hydrolysis

Elena V. Ivanova[1], Peter M. Kolosov[1], Berry Birdsall[2], Geoff Kelly[2], Annalisa Pastore[2], Lev L. Kisselev[1] and Vladimir I. Polshakov[3]

1 Engelhardt Institute of Molecular Biology, Russian Academy of Sciences, Moscow, Russia
2 Division of Molecular Structure, National Institute for Medical Research, London, UK
3 Center for Magnetic Tomography and Spectroscopy, M. V. Lomonosov Moscow State University, Russia

The eukaryotic class 1 polypeptide chain release factor is a three-domain protein involved in the termination of translation, the final stage of polypeptide biosynthesis. In attempts to understand the roles of the middle domain of the eukaryotic class 1 polypeptide chain release factor in the transduction of the termination signal from the small to the large ribosomal subunit and in peptidyl-tRNA hydrolysis, its high-resolution NMR structure has been obtained. The overall fold and the structure of the β-strand core of the protein in solution are similar to those found in the crystal. However, the orientation of the functionally critical GGQ loop and neighboring α-helices has genuine and noticeable differences in solution and in the crystal. Backbone amide protons of most of the residues in the GGQ loop undergo fast exchange with water. However, in the AGQ mutant, where functional activity is abolished, a significant reduction in the exchange rate of the amide protons has been observed without a noticeable change in the loop conformation, providing evidence for the GGQ loop interaction with water molecule(s) that may serve as a substrate for the hydrolytic cleavage of the peptidyl-tRNA in the ribosome. The protein backbone dynamics, studied using ^{15}N relaxation experiments, showed that the GGQ loop is the most flexible part of the middle domain. The conformational flexibility of the GGQ and 215–223 loops, which are situated at opposite ends of the longest α-helix, could be a determinant of the functional activity of the eukaryotic class l polypeptide chain release factor, with that helix acting as the trigger to transmit the signals from one loop to the other.

Termination of translation, one of the most complex stages in protein biosynthesis, is regulated by the co-operative action of two interacting polypeptide chain release factors, eukaryotic class 1 polypeptide chain release factor (eRF1) and eukaryotic class 2 polypeptide chain release factor 3 (eRF3). The roles of these

termination factors have been validated *in vitro* in a completely reconstituted eukaryotic protein synthesis system [1]. The two major functions of eRF1 are: (a) recognition of one of the three stop codons, UAA, UAG or UGA, in the decoding center of the small ribosomal subunit; and (b) participation in the subsequent hydrolysis of the ester bond in peptidyl-tRNA. eRF3 is a ribosome- and eRF1-dependent GTPase that is encoded by an essential gene, and its role in translation termination requires further elucidation [2].

The human eRF1 structure, in the crystal [3] and in solution [4], consists of three domains. The N-terminal domain is implicated in stop codon recognition [5–14]. The role of the middle (M) domain will be described in detail below. The C domain of eRF1 interacts with the C domain of eRF3 [15–18], and the binding of both factors is essential for fast kinetics of the termination of translation [1]. However, in a simplified *in vitro* assay for measuring polypeptide chain release factor (RF) activity, eRF1 deprived of the C domain still retains its RF activity [19].

The most characteristic feature of the M domain is the presence of the strictly conserved GGQ motif [20]. In prokaryotes, there are two polypeptide release factors called RF1 and RF2, which are functionally equivalent to eRF1 in eukaryotes [21,22]. In the *Escherichia coli* ribosome, the GGQ motif of RF1 or RF2 is located at the peptidyl transferase center (PTC) on the large ribosomal subunit, as revealed by cryo-electron microscopy [23,24], crystal structure data [25], and biochemical data [26]. It was suggested [26] and shown by cryo-electron microscopy [23,24] and X-ray diffraction [25] that RF2 undergoes gross conformational changes upon binding to the ribosome that could possibly allow the loop containing the GGQ motif to reach the PTC of the ribosome and to promote peptidyl-tRNA hydrolysis. A significant conformational change was also suggested for eRF1 [27] and demonstrated by molecular modeling [28]. It has been suggested that the GGQ motif, being universal for all class 1 RFs and critically important for functional activity of both prokaryotic and eukaryotic class 1 RFs, should be involved in triggering peptidyl-tRNA hydrolysis at the PTC of the large ribosomal subunit [20]. The three-domain structure of eRF1, with the shape of the protein resembling the letter 'Y', partly mimics the 'L'-shape of the tRNA molecule, and the M domain of eRF1 is equivalent to the acceptor stem of a tRNA [29]. It has also been suggested that the GGQ motif is functionally equivalent to the universal 3′-CCA end of all tRNAs [20]. The evidence in support of this hypothesis is growing [25].

Mutations of either Gly in the GGQ triplet were shown to abolish the peptidyl-tRNA hydrolysis activity of human eRF1 *in vitro* [20,30], of yeast eRF1 *in vivo* [3], and of *Es. coli* RF2 both *in vivo* and *in vitro* [31,32]. For instance, GAQ mutants of both RF1 and RF2 are four to five orders of magnitude less efficient in the termination reaction than their wild-type counterparts, although their ability to bind to the ribosome is fully retained upon mutation [31]. Thus, the toxicity of these mutants for *Es. coli in vivo* can be explained by their competitive inhibition at the ribosome-binding site [32].

Together, the M and C domains of human eRF1, in the absence of the N domain, are able to bind to the mammalian ribosome and induce GTPase activity of eRF3 in the presence of GTP [33].

The previously determined relatively low-resolution crystal structure [3] (2.7 Å highest resolution) of the M domain was unable to provide all the necessary details of the molecular mechanism of the termination of translation in the ribosomal PTC. It still remains unclear how a stop signal can be transmitted from the small to the large ribosomal subunit, and how the M domain participates in hydrolysis of the peptidyl-tRNA ester bond. The aim of this work was to determine the structure and obtain dynamic information on the M domain of human eRF1 in solution, which may help to clarify these important unanswered questions.

Results

Resonance assignment

^{1}H, ^{13}C and ^{15}N chemical shift assignments were made for essentially all the observed protein backbone amide resonances. More than 95% of all observed side-chain ^{1}H, ^{13}C and ^{15}N chemical shifts were also determined. However, at 298 K, backbone signals from residues 177–187, the loop containing the GGQ motif, could not be detected. For example, no amide signals attributable to G181, G183 and G184 were observed in the relatively empty Gly region of the ^{15}N,^{1}H-heteronuclear single quantum coherence spectroscopy (HSQC) spectrum at this temperature. At lower temperatures (278 K), these amide signals can be detected in the ^{15}N-HSQC spectra (Fig. 1A), and the assignments were confirmed by three-dimensional experiments correlating amide HN and Cα signals (HNCA) and ^{15}N-NOESY-HSQC experiments. The absence of amide signals at 298 K appears to be due to fast exchange of these amide protons with water. An alternative mechanism of line broadening could be related to conformational exchange in the GGQ loop, e.g. the
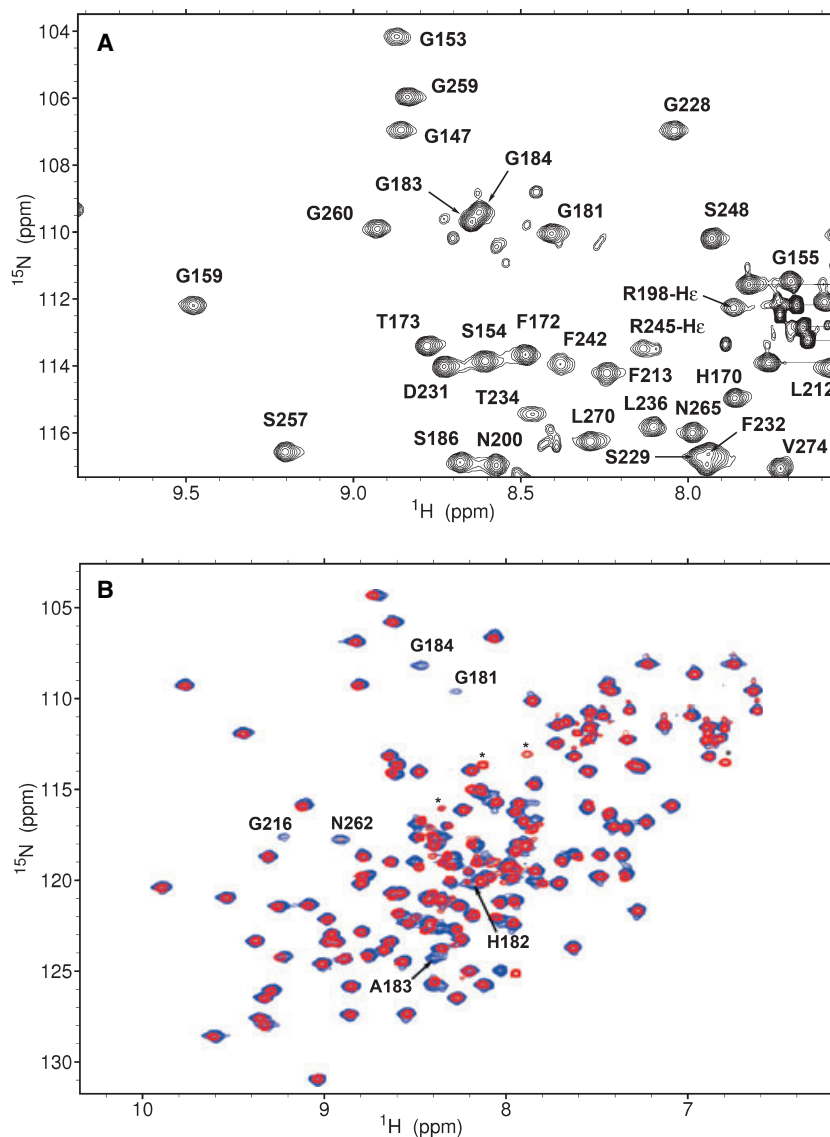
Fig. 1. ^{1}H,^{15}N-HSQC spectra of the M domain of human eRF1. The numbering of the residues corresponds to that of the full eRF1 protein. (A) The Gly region of the ^{1}H,^{15}N-HSQC spectrum of the M domain of human eRF1 recorded at 278 K. (B) The superposition of the ^{1}H,^{15}N-HSQC spectra of wild-type (red) and G183A mutant (blue) of the M domain of human eRF1 recorded at 298 K. Clearly visible in blue are the residues that are absent in the spectrum of the wild-type protein due to fast exchange with water.

cis/trans interconversion within the Gly residues [34]. However, in this case, one can expect to detect similar behavior of the signals from labile and nonlabile protons. A series of ^{13}C-HSQC spectra recorded in the temperature range between 5 °C and 30 °C showed that the line widths of the Hα signals of the Gly residues named above do not change very much. These facts unambiguously confirm fast exchange of the backbone amide protons in the GGQ loop with water at 298 K. Unlike the backbone amide signals, the side-chain signals of Q185 were observed at 298 K and assigned as the only remaining unassigned pair of H$_2$N.

At 278 K, residues Gly181, Gly183 and Gly184 are observed in the ^{15}N-HSQC spectrum, and each

appears as a group of signals with different intensities and slightly different chemical shifts (Fig. 1A), indicating that this part of the GGQ loop exists as a mixture of several conformational states similar to that found for some other proteins [35,36]. The exchange between these conformational states happens at a relatively slow rate (slower than $\sim 1\ s^{-1}$ as estimated from line shape analysis). These small peaks cannot be assigned to the breakdown protein species, because in that case many other peaks in the protein spectrum should have similar minor satellites. Additionally, for several such peaks, sequential and intraresidue correlations were found in the HNCA and ^{1}H,^{15}N-NOESY-HSQC spectra, confirming the assignment of these satellite peaks to residues G181, G183 and G184. The existence of a

protein fragment in multiple conformational states reflects the very complex dynamic behavior of the GGQ loop.

Effect of G183A mutation

A comparison of the spectra recorded at 298 K for the wild-type M domain of human eRF1 and the G183A mutant (where the first Gly residue in the GGQ motif is replaced by Ala) shows that the chemical shifts of the vast majority of HN resonances are virtually identical in these two species (Fig. 1B). There are, however, several important differences. In the ^{15}N-HSQC spectrum of the G183A mutant, as well as the new signal from the backbone amide of Ala183 (the mutation point), one now can also observe signals from the neighboring residues His182, Gly184 and Gly181, which were all absent in the ^{15}N-HSQC spectrum of the wild-type protein recorded at 298 K. Interestingly, the chemical shifts of these resonances in the G183A mutant are very similar to those detected at lower temperature in the wild-type protein, indicating that the mutation has little (if any) effect on the conformation of the GGQ loop. At the same time, however, the G183A mutation results in a decrease in the rate of exchange of the backbone amide protons with water, and the NMR signals from the mutant loop residues are visible at higher temperature (298 K). Surprisingly, two other signals (Gly216 and Asn262) that were absent in the ^{15}N-HSQC spectrum of the wild-type M domain of eRF1 recorded at 298 K are now visible in the spectrum of the G183A mutant.

Structure determination

A family of 25 NMR structures was determined on the basis of 2338 experimental restraints measured at 278 K and 298 K (Tables 1–3). This work made use of standard double-resonance and triple-resonance NMR methods applied to unlabeled, ^{15}N-labeled and ^{15}N/^{13}C-labeled samples of the M domain of eRF1. For most of the protein residues, the number of NOEs per residue is between 20 and 40; however, this number is significantly lower for residues 178–184, which are near the GGQ motif, and for several other loop region residues.

The statistics of the final ensemble are given in Tables 1–3, and the superposition of the final calculated family is presented in Fig. 2A (backbone atoms of the M domain of the human eRF1 crystal structure [3] are also shown in red for comparison). The NMR structures had the lowest target-function values, no distance restraint violations greater than 0.2 Å, and no

Table 1. Restraints used in the structure calculation of the M domain of human eRF1.

Total NOEs	1975
Long range ($|i–j| > 4$)	428
Medium ($1 < |i–j| \leq 4$)	236
Sequential ($|i–j| = 1$)	448
Intraresidue	863
H-bonds	12
Total dihedral angles	214
Phi (φ)	96
Psi (ψ)	97
Chi1 (χ1)	21
Residual dipolar couplings	
N–H	120
$C_a–H_a$	5

Table 2. Restraint violations and structural statistics for the calculated structures of the M domain of human eRF1 (for 25 structures). No NOE or dihedral angle violations are above 0.2 Å and 10°, respectively.

Average rmsd	$<S>$[a]	S_{rep}
From experimental restraints		
Distance (Å)	0.020 ± 0.001	0.020
Dihedral (°)	4.369 ± 0.204	4.397
Residual dipolar coupling (Hz)	0.028 ± 0.002	0.030
From idealized covalent geometry		
Bonds (Å)	0.008 ± 0.0002	0.008
Angles (°)	1.377 ± 0.027	1.335
Impropers (°)	1.903 ± 0.055	1.867
% of residues in most favorable region of Ramachandran plot	89.9	89.9
% of residues in disallowed region of Ramachandran plot	0.0	0.0

[a] $<S>$ is the ensemble of 25 final structures; S_{rep} is the representative structure, selected from the final family on the criterion of having the lowest sum of pairwise rmsd for the remaining structures in the family.

Table 3. Superimposition on the representative structure (Table 2).

Backbone (C, Cα, N) rmsd of residues 142–275	0.87 ± 0.36
All heavy-atom rmsd of residues 142–275	1.14 ± 0.26
Backbone (C, Cα, N) rmsd of the protein without unstructured loop residues 178–186	0.70 ± 0.34
Backbone (C, Cα, N) rmsd of the core region of protein (residues 142–174, 200–275)	0.38 ± 0.07

dihedral angle violations > 10°. The representative structure (first model in the family of 25 NMR structures) was selected from the calculated family, as the structure closest to the average structure and giving the lowest sum of pairwise rmsd values for the remainder of the structures in the family. The rmsd of the calculated family from the representative structure is

Fig. 2. The solution structures of the M domain of human eRF1. (A) The stereo view of the ensemble of the final 25 calculated structures superimposed on heavy backbone atoms (Ca, N and C). The poorly structured GGQ loop region (residues 175–189) was excluded from the superposition. The crystal structure of the M domain of the human eRF1 [3] is superimposed on the same set of atoms in the representative solution structure and is shown in red. (B) The topology of the M domain of human eRF1 and the secondary structure elements displayed using MOLMOL [65]. (C) Representative structure of the GGQ loop of the M domain of human eRF1.


below 0.9 Å for the backbone heavy atoms. However, most of this value originated from the large contribution from the poorly structured GGQ loop. Excluding these residues, 175–189, the rmsd for heavy atoms of the protein backbone is less than 0.4 Å. In the Ramachandran plot analysis, 89.9% of the residues in the whole NMR family were found in the most favored regions and none in the disallowed regions.

Structure analysis

The conformations of the backbone and side-chains of the M domain of human eRF1 are well defined except for the residues (175–189) in the GGQ loop. The backbone conformation of this loop is discussed below in the section 'Geometry of the GGQ loop'.

The topology of the M domain of human eRF1 can be described as a β-core constructed of a sheet formed from five β-strands (both parallel and antiparallel), surrounded by four helices, α1–α4 (Fig. 2B). Strand β3 has a substantial twist at residues 168–169. The longest α-helix (α1) starts at the end of the GGQ loop and has a bend at residues 195–196. There are also several loops of various lengths, the longest of which is the GGQ loop. Another loop of interest starts at the C-terminus of helix α1 and connects with β-strand β4, and has a conformation similar to two short antiparallel β-strands with a turn at residue Gly216.

The solution structure of the M domain of human eRF1 presented in this work shows considerable similarity to the crystal structure of the M domain of the same protein [3], but it is far from identical (Fig. 2A). The rmsd of the superposition of the heavy backbone atoms (Cα, N, O and C) of the family of 25 NMR structures onto the crystal structure for the whole M domain (residues 140–275) is 3.8 ± 0.2 Å. An analogous rmsd value for the superposition of the more structured part of the protein (residues 144–174 and 200–272) is much lower, 2.7 ± 0.1 Å. The relatively large value originates mainly from the differences in orientation of the loops and helices, as discussed later.
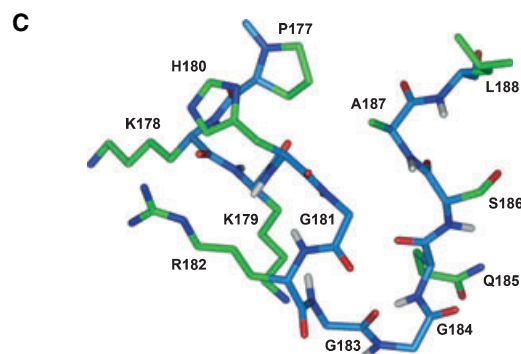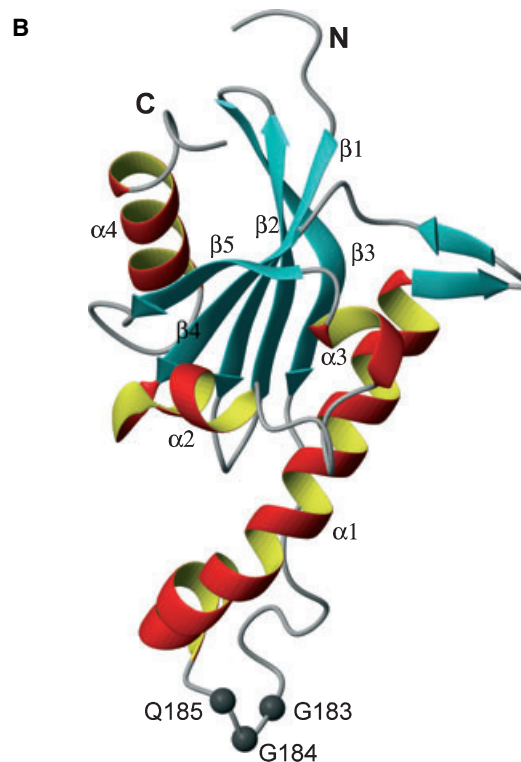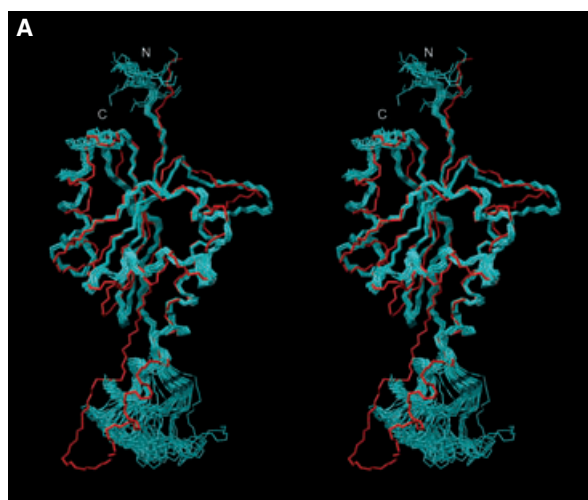
Geometry of the GGQ loop

The GGQ loop is the most disordered part of the protein structure (Fig. 2A). However, this loop contains the most important functional motif and should therefore be characterized in detail. The selection of a representative conformation for the GGQ loop (residues 177–188) was derived from an analysis of all the conformations found in the family of calculated NMR structures (Table 4). This was done by determining a representative value for each backbone torsion angle (ϕ and ψ) and each side-chain torsion angle χ_1. In many cases, these representative values were close to the mean value of the torsion angle in the family. In other cases, when two or several clusters of torsion angle values were observed, the value from the most populated cluster was taken as the representative value. These values were then used to build up a model of the 177–188 loop (Fig. 2C). There are no interatomic clashes in this model. The rmsd value for the superposition of the heavy backbone atoms (Ca, C, N and O) of this model on the corresponding part of the family of calculated NMR solution structures is 1.32 ± 0.35 Å. The rmsd decreases to 1.01 ± 0.16 Å when it is superimposed on 13 selected structures from the family of 25 NMR structures. The rmsd is similar, 1.02 Å, for the superposition on the representative structure of the family, and it has a minimum value, 0.76 Å, for one member of the NMR family.

Backbone dynamics

Figure 3 presents the experimentally obtained relaxation rates R_1 (longitudinal or spin–lattice relaxation rate) and R_2 (transverse or spin–spin relaxation rate) and NOE values for the amide ^{15}N nuclei measured at 278 K, and the calculated values of the order parameter S^2 reflecting the amplitude of ps–ns bond vector dynamics. The relaxation parameters were obtained using the model with an axially symmetric
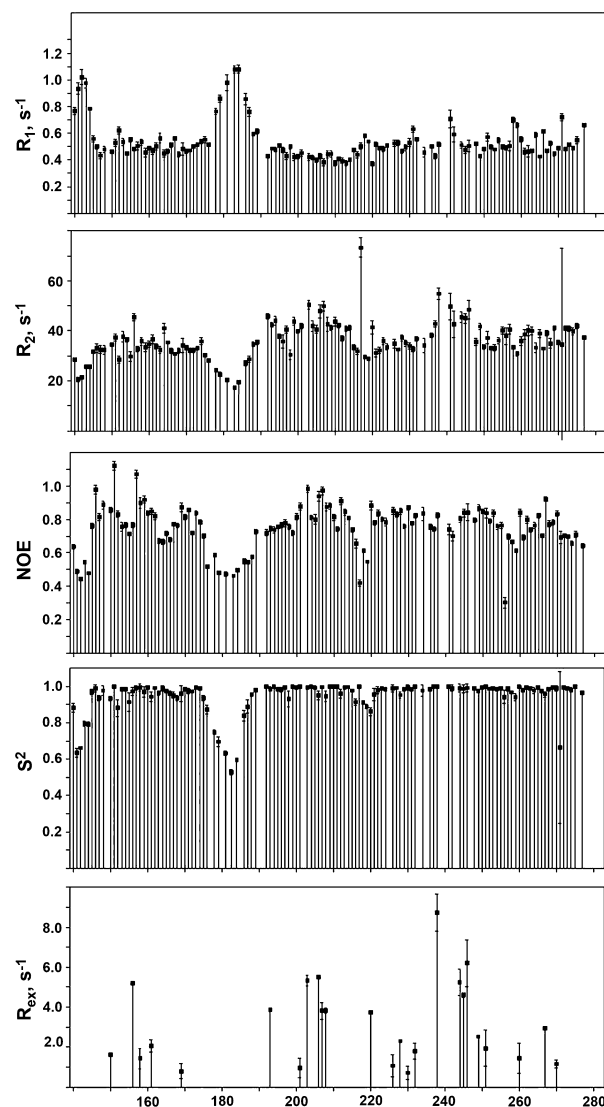
Fig. 3. The relaxation parameters of the amide ^{15}N spin of each residue measured at 18.7 T (800 MHz proton resonance frequency) and 278 K. (A) The longitudinal relaxation rate, R_1. (B) The transverse relaxation rate, R_2. (C) The heteronuclear ^{15}N,^{1}H-steady-state NOE value. (D) The order parameter, S^2, determined by model-free analysis with an assumption of axially symmetric anisotropic rotational diffusion. (E) The chemical exchange rate R_{ex}.
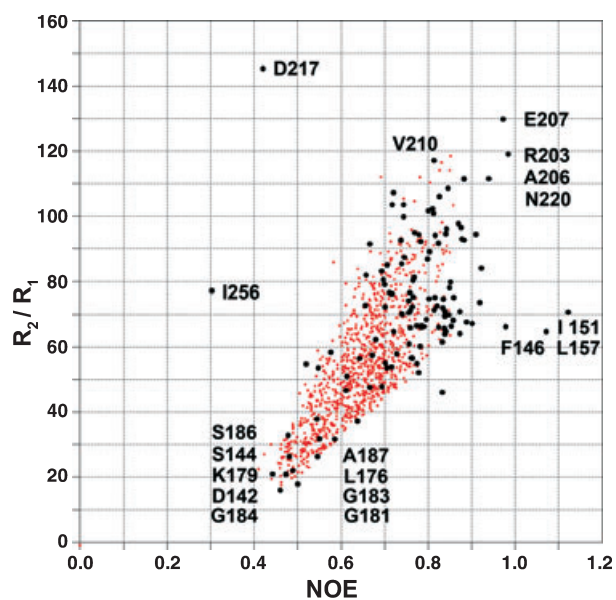
Table 4. The geometry of the GGQ loop in the family of 25 NMR structures of the M domain of human eRF1.

Residue	Ranges of torsion angles in whole family[a]			Torsion angles in representative structure		
	ϕ	ψ	χ_1	ϕ	ψ	χ_1
Pro177	-19 ± 3	161 ± 6	-48 ± 2	-20	160	-48
Lys178	-72 ± 14	-40 ± 11	-90 ± 21	-64	-43	-60
Lys179	-77 ± 13	128 ± 12	-63 ± 30	-70	130	-60
His180	-128 ± 17	48 ± 68	-128 ± 93	-120	45	180
Gly181	80 ± 51	-4 ± 13		90	0	
Arg182	-53 ± 58	-22 ± 46	-62 ± 105	-63	-40	-60
Gly183	-66 ± 104	-135 ± 73		-87	-170	
Gly184	-53 ± 44	-23 ± 16		-63	-35	
Gln185	-90 ± 23	135 ± 7	-110 ± 17	-75	135	-60
Ser186	-68 ± 5	148 ± 4	0 ± 110	-73	150	[b]
Ala187	-64 ± 1	-41 ± 2		-64	-42	
Leu188	-64 ± 1	-42 ± 1	-110 ± 23	-64	-42	[b]

[a] The mean value in the family of 25 structures and the SD. [b] There is no preferred conformation of the side-chain in the family.

diffusion tensor. The order parameter is smallest (that is, for the most typical types of internal motions, the amplitude of such motions is largest) for residues 176–187 and also the N-terminal residues. The chemical exchange contribution to the transverse relaxation rate R_{ex} (conformational exchange contribution to R_2) is also shown in Fig. 3. The relaxation parameters were obtained using the model with an axially symmetric diffusion tensor. The average correlation time $[1/(2D_{\parallel} + 4D_{\perp}]$ was 20.8 ± 0.8 ns, and the ratio of the principal axis of the tensor $(D_{\parallel}/D_{\perp})$ was 1.8 ± 0.1. It is necessary to note that the model that allows the most successful fit of the experimental data is based on two internal motions that are faster than the overall rotational tumbling [37]. Figure 4 illustrates the convergence of the simulated data (red spots) with most of the experimental data (black circles). The synthetic data were calculated assuming the existence of relatively slow internal motions, occurring with a 1.1 ± 0.1 ns correlation time and an order
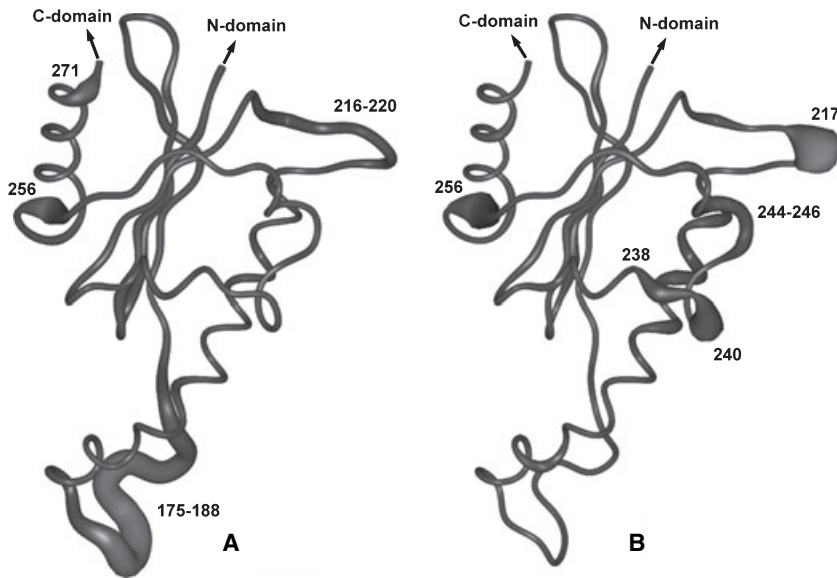
parameter between 0.5 and 1.0, against a background of faster motions occurring with a correlation time below 20 ns and an order parameter between 0.8 and 1.0. This was calculated without the assumption of conformational line broadening. The residues that exhibit slow conformational rearrangements occurring on a millisecond time scale and leading to an increase in the transverse relaxation rate can be found in a region outside and to the top of the synthetic dataset (Fig. 4). The most atypical residues in this group are D217, I256 and V210. Residues on the right side of this plot (i.e. with the largest NOE values) mostly come from the rigid protein core. Figure 4 provides a clear and useful illustration of the dynamic behavior of the protein.

Figure 5 shows a ribbon representation of the M domain with the cylindrical radius proportional to the order parameters S^2 (A) and R_{ex} (B). Interestingly, ignoring the trivial case of the N-terminal residues, the two most flexible loop regions in the M domain are situated on the two opposite sides of the long helix, $\alpha 1$ (Figs 2B and 5). The GGQ loop exhibits motions occurring with a ~ 1 ns correlation time, whereas the loop composed of residues 215–223 undergoes motions on both the nanosecond and millisecond time scales. Another flexible part of the protein that undergoes motions on both the fast and slow time scales (indicative residue I256) is the beginning of the helix $\alpha 4$, which connects to the C domain of human eRF1.

Discussion

The family of class 1 release factors

The alignment of the amino acid sequences of the M domains of eRF1s and aRF1s (archaeal RFs) from diverse organisms, including the evolutionarily distant eRF1s from lower eukaryotic organisms with variant genetic codes, such as *Stylonichia* and *Euplotes*, is shown in Fig. 6. The sequences between Leu176 and Ala210 (human eRF1 numbering) are highly conserved and contain, apart from the invariant GGQ motif, some other residues near this motif that are also completely conserved among all species, including members of the archaea, namely Pro177, Lys179 and Ser186 in the loop region, and Arg189, Phe190 and Leu193 at the beginning of the $\alpha 1$ helix. The highly conserved Gly residues in positions 163, 183, 184 and 228 most likely have a topology-forming role, allowing the protein backbone to have a specific geometry. Several other highly conserved residues may have a functional role by forming an interface for protein–RNA binding.

Fig. 4. The distribution of the experimental (black dots) and simulated (small red squares) ratios of relaxation rates R_2/R_1 vs. the heteronuclear ^{15}N,^{1}H-NOE values. The data were simulated at 800 MHz proton resonance frequency using Clore's extension of the Lipari and Szabo model [37]. The axial symmetry with the ratio $D_{\parallel}/D_{\perp}$ of the principal axis of the tensor was 1.8 ± 0.1; the value of effective overall correlation time $1/(2D_{\parallel} + 4D_{\perp})$ was 20.8 ± 0.8 ns; the values of the order parameter S^2_{slow} were between 0.5 and 1.0; the values of the order parameter S^2_{fast} were between 0.8 and 1.0; the values of the internal motion correlation times τ_{slow} were between 1 and 1.1 ns; and the values of the internal motion correlation times τ_{fast} were between 0 and 20 ps.

Fig. 5. Ribbon representation of the backbone of the M domain of human eRF1. The variable radius of the cylinder is proportional to the dynamic properties of the protein residues. (A) Fast motions (on a picosecond to nanosecond time scale). The thickness of the backbone ribbon is proportional to the value of $1 - S^2$; the minimal thickness corresponds to the value $S^2 = 1$, and the maximum to $S^2 = 0.5$. (B) Slow conformational rearrangements (occurring on a millisecond time scale). The thickness of the backbone ribbon is proportional to the value of R_{ex}; the minimal thickness corresponds to the value $R_{ex} = 0$, and the maximum to $R_{ex} = 10$.
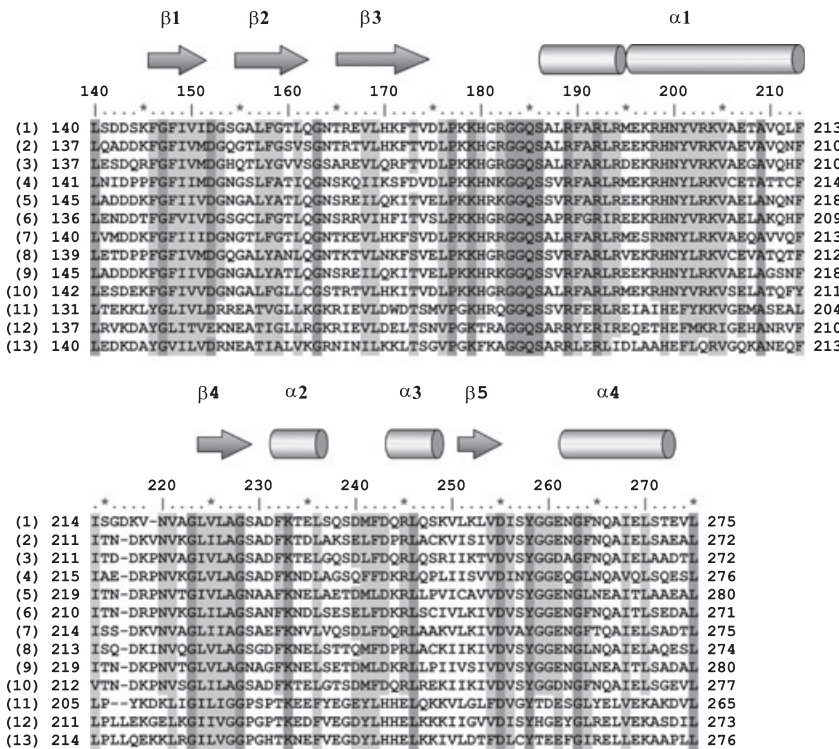
Fig. 6. Sequences of the M domains of eRF1/aRF1 from *Homo sapiens* (1), *Saccharomyces cerevisae* (2), *Schizosaccharomyces pombe* (3), *Paramecium tetraurelia* (4), *Oxytricha trifallax* (5), *Euplotes aediculatus* (6), *Blepharisma americanum* (7), *Tetrahymena thermophila* (8), *Stylonychia mytilus* (9), *Dictyostelium discoideum* (10), *Archaeoglobus fulgidus* (11), *Pyrococcus abyssi* (12) and *Methanococcus jannaschii* (13), as aligned using BLAST [71], with minor manual corrections. Highly and completely conserved residues of RFs are indicated by dark and light gray, respectively. Identified secondary structure elements in the M domain of human eRF1 are shown above the sequence. The numbering above the sequence corresponds to human eRF1.

The high level of the alignment similarity suggests that the tertiary structure of the M domain is well conserved in both eukaryotic and archaeal RFs.

The high degree of conservation of the GGQ-containing fragment of the M domain is most likely to be associated with its role in triggering peptidyl-tRNA hydrolysis. As the ribosomal PTC is mostly composed of rRNA, which in turn is also highly conserved across species [38–40], the conservation of the GGQ-containing fragment is likely to be associated with its binding to the conserved RNA sequences.

Comparison with the crystal structure of human eRF1

The most noticeable difference between the crystal structure of the M domain in the whole protein and the solution structure of the separated individual

M domain as seen in Fig. 2A is the orientation of the GGQ loop and its connection to helix α1. Our confidence in the accuracy of the determination of the orientation of the flexible GGQ loop in solution is based on the extensive use of residual dipolar coupling restraints, both $^1D(^{15}N,^1H)$ and $^1D(^{13}C,^1H)$, that show good agreement between experimental and calculated values of these parameters. There are three possible reasons for the differences between the crystal and the solution structures of the M domain. First, the orientation of the loop may change, due to crystal-packing effects. Second, the coordinates of the GGQ loop may not be determined by the X-ray data sufficiently well, because of the relatively low resolution and the flexibility of the GGQ loop. It is of note that about 2.8% of the eRF1 residues in the crystal structure were found in disallowed regions of the Ramachandran plot [3], which indicates that experimental problems may have resulted in a decrease in the overall quality of the structure. Finally, the C and N domains may have structural influences on the M domain within the whole eRF1 protein.

The pairwise comparison of the solution structures with the X-ray crystal structure of the M domain using the superposition of five-residue fragments (Fig. 7) shows that the local geometry of regions 177–184, 194–195, 213–219, 237–245 and 258–260 is different. All these regions, except 194–197, correspond to loops that connect regular secondary structure elements. Residues 194–197 are situated at the bend in helix α1, and are not observed in the crystal structure of human eRF1 [3]. Therefore, the differences between the crystal and solution structures arise mainly from changes in the orientations of the loops and α-helices relative to the β-core.

Effect of mutations

The mutation of either Gly residue in the GGQ motif of class 1 RFs has been shown to abolish the RF activity both *in vivo* and *in vitro*. The G183A mutant of human eRF1 was totally inactive in peptidyl-tRNA hydrolysis [20], and it has been proposed that this mutation alters the structure of the GGQ loop [1].

However, the replacement of Gly183 by an Ala has only minor effects on the chemical shifts of signals from the vast majority of the residues of the M domain (Fig. 1B). This is strong evidence that there is no substantial change in the conformation of the protein or in the distribution of the conformational ensemble of the GGQ loop. In contrast to this lack of effect on the conformation, the G183A mutation has a drastic effect on the exchange of amide protons with water.

Fast exchange with water of GGQ loop amide protons

It was noted above that many of the residues in the GGQ loop were not detected in the NMR spectra of the wild-type M domain at room temperature, due to fast exchange with water. Such fast exchange of the amide proton with water can be caused by several possible mechanisms. These include: (a) coordination of a water molecule(s) involved in subsequent exchange with amide proton, facilitated by appropriate orientation of HN bonds relative to the CO bond [41]; and (b) the local pH being above 8 and thereby allowing the HNs to exchange rapidly via base catalysis [42].

The GGQ loop region has a predominant positive charge, and this may have implications for the possible binding of the protein to rRNA [3]. One of the
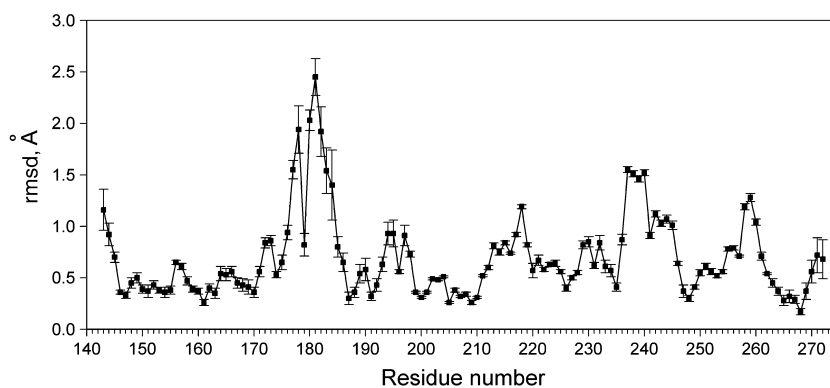
Fig. 7. A plot of the calculated rmsd for the displacements over the backbone atoms (Cα, C and N) calculated from the pairwise superimposition of five-residue segments of the crystal structure on the equivalent segments of each member of the family of the solution structure of the M domain of human eRF1. The resulting rmsd values (*y*-axis) and their deviations through the 25 NMR structures are shown for the central residue of the five-residue segments (*x*-axis).

possible consequences of this charge imbalance could be an increase in the local pH. However, the fact that the G183A mutation significantly decreases the exchange rate of the amide protons in the loop region indicates that a higher local pH is unlikely to be the reason for the fast exchange, as the replacement of one neutral residue by another without a conformational change cannot substantially influence the distribution of the local potential. Therefore, most probably, the observed effect relates to the coordination of a water molecule(s) in the GGQ loop and its involvement in catalysis of amide proton exchange.

The possible water coordination to the GGQ loop may facilitate an understanding of the mechanism of peptidyl-tRNA hydrolysis. It has been suggested that the glutamine side-chain in the GGQ minidomain acts to coordinate the substrate water molecule that performs the nucleophilic attack on the peptidyl-tRNA ester bond and that the conserved adjacent Gly and neighboring basic residues facilitate contact with the phosphate backbone of either rRNA and/or the acceptor stem of the P site tRNA [3]. Although this hypothesis has not been supported by any experimental data [30,43–45], one can propose, on the basis of the current observations, that the protein backbone of the GGQ loop could be responsible for the water molecule coordination.

Dynamic properties of the M domain

The dynamic behavior of the M domain has several important features. First of all, the most flexible region is the GGQ loop, which is also the most important functionally. It undergoes not only very fast (picosecond to nanosecond time scale) but also relatively slow conformational rearrangements, occurring on a millisecond to second (and possibly slower) time scale. High mobility is a characteristic of many RNA- and DNA-binding proteins [46–48], and may facilitate easier positional rearrangement of the protein during the docking to the binding site on the ribosome or other ligands. Strikingly, the second most flexible part of the protein (if one does not take into account the N-terminal region of the M domain) is the loop situated on the other end of helix α1 from the GGQ motif (Fig. 5). This loop (residues 215–223) undergoes both fast (with a correlation time of about 1 ns) and slow (millisecond time scale) motions. There are two possible functional implications of the behavior of this loop. The first is the facilitation of the conformational rearrangements and the maintenance of the conformational plasticity for effective binding of the protein to the ribosome. The second, and more plausible, is that

the loop is situated at the interface between the M and N domains of eRF1, and this flexibility may be involved in transduction of the signal from the N-terminal domain, upon the recognition of the stop codon, to the M domain for subsequent initiation of the hydrolysis of peptidyl-tRNA ester bond. Two possible models of signal transduction may be considered. The first model assumes that the signal is transmitted directly through the body of eRF1 from the N domain to the GGQ loop of the M domain located in the PTC. The second model postulates that rRNA(s) could mediate the signal transduction through the following schematic chain: N domain → 18S rRNA → 28S rRNA → M domain → GGQ → PTC-peptidyl-tRNA. No evidence is available at present that favors either model; however, the flexibility of the M domain may be implicated in both models. The long and relatively dynamically rigid helix α1 could serve as a trigger that facilitates the conformational change in one loop consequent to a change at the other loop.

Interestingly, the short loop at the interface between strand β6 and the C-terminal helix α3 also exhibits the two types of motion – slow conformational rearrangement occurring on a millisecond time scale, and relatively fast motions (with ~1 ns correlation time). This slow motion was detected from the large increase of the transverse relaxation rate of residue I256, occurring at the same time as the fast motions. Helix α3 connects the M domain with the C domain of eRF1, and the motions of this short loop could be a reflection of the absence of the interacting C domain in this construct.

Experimental procedures

Sample preparation

To construct the pET-MeRF1 vector for expression of the human eRF1 fragment encoding the M domain with the C-terminal His6-tag fusion, a PCR fragment derived from pERF4B [6] was inserted between the *Nde*I and *Xho*I sites of pET23b (Novagen, Madison, WI, USA). The M domain (residues 142–275 of human eRF1) was overproduced in *Es. coli* strain BL21(DE3) in M9 minimal medium. For ^{13}C and/or ^{15}N labeling [$^{13}C_6$]D-glucose and/or $^{15}NH_4Cl$ (Cambridge Isotope Laboratories Inc., Andover, MA, USA) were used as a sole carbon and/or nitrogen source in M9 minimal medium. The His6-tagged M domain of human eRF1 was isolated and purified using affinity chromatography on Ni^{2+}–nitrilotriacetic acid agarose (Qiagen, Germantown, MD, USA). Peak fractions were dialyzed against 20 mM potassium phosphate buffer (pH 6.9) and 50 mM NaCl, and then purified by cation exchange chromatography using HiTrap SP columns (Amersham Pharmacia Biotech,

Piscataway, NJ, USA) in 20 mM potassium phosphate buffer (pH 6.9). Purified protein was concentrated to approximately 1 mM. The final purity of the sample was about 98%, as determined by SDS/PAGE.

The samples for NMR at approximately 1 mM concentration were prepared in either 95% H_2O/5% D_2O or in 100% D_2O and 20 mM potassium phosphate and 50 mM KCl (pH 7.0). Typically, the volume of the samples was 380 μL, in Shigemi microcell NMR tubes.

NMR spectroscopy

All spectra were acquired between 5 °C and 30 °C on a Varian (Palo Alto, CA, USA) INOVA 600 and 800 MHz NMR spectrometer equipped with triple-resonance z-gradient probes and a Bruker (Karlsruhe, Germany) AVANCE 600 MHz spectrometer equipped with a triple-resonance cryoprobe. Spectra were processed by NMRPIPE [49], and analyzed using SPARKY (from Goddard and Kneller, San Francisco, CA, USA; http://www.cgl.ucsf.edu/home/sparky) and AUTOASSIGN [50]. Sequential assignments for the backbone were obtained [51] using the following three-dimensional (3D) spectra: HNCO, HNCA, HN(CO)CA, HNCACB, CBCA(CO)NH, HNHAHB and HBHA(CO)NH [52]. Aliphatic side-chain resonances were derived from 3D HCCH-TOCSY, HNHB, ^{1}H,^{15}N-NOESY-HSQC and ^{1}H,^{13}C-NOESY-HSQC spectra. Distance restraints for structure calculations were obtained from the 3D ^{15}N- and ^{13}C-separated NOESY spectra recorded at 25 °C and 5 °C with 100 ms mixing time.

Residual dipolar coupling measurements were performed using ternary poly(ethylene glycol) ether/alcohol/buffer mixtures as described by Ruckert & Otting [53]. Residual dipolar coupling $^{1}D_{NH}$ values were obtained from inphase antiphase-HSQC spectra [54] recorded in ~5% w/w n-dodecylpenta(ethylene glycol)/hexanol media at 298 K (59 values) and in 5% w/w n-octyl-penta(ethylene glycol)/octanol media at 283 K (61 values), and corresponding $^{1}J_{NH}$ values were measured in anisotropic solution at the same temperature.

Spectra for ^{15}N longitudinal relaxation rates R_1, transverse relaxation rates R_2 and ^{15}N,^{1}H-heteronuclear NOE values were collected on the 1 mM ^{15}N-labeled M domain eRF1 sample at 278 K with a Varian INOVA 800 MHz NMR spectrometer, and at 293 K with a Varian INOVA 600 MHz NMR spectrometer, using the pulse sequences modified from those described by Kay *et al.* [55] to compensate for cross-correlation effects [56].

Structure calculation and refinement

The NOE cross-peaks were integrated, and corresponding proton–proton distances were grouped into four ranges with upper limits of 2.5 Å, 3.5 Å, 4.5 Å and 5.5 Å.

The ranges for backbone torsion angles φ and ψ were derived from the values of $^{13}C_{\alpha}$, $^{13}C_{\beta}$, $^{13}C'$, $^{1}H_{\alpha}$ $^{1}H_N$ and ^{15}N

chemical shifts and the software TALOS [57]. Stereospecific assignments for Hβs and pro-R/pro-S methyl groups of Val and Leu residues, together with the values of torsion angles χ_1, were obtained using the program ANGLESEARCH [58].

To generate an initial structure, a set of unambiguously assigned NOEs was submitted to ARIA, and further assigned NOEs were obtained via an iterative procedure [59] using the ARIA-CNS crystallography and NMR system [60]. Donors of hydrogen bonds − slowly exchanging amide protons − were detected in the NOESY spectrum acquired in D_2O. Acceptors of hydrogen bonds were identified among the nearby carbonyl groups in the final stages of structure calculations. Two distance restraints were employed for each hydrogen bond (r_{NH-O} < 2.4 Å and 2.4 Å < r_{N-O} < 3.4 Å). In total, 12 hydrogen bonds (24 restraints) were used to refine the structure.

For refinement of the structure, experimentally determined distance, torsion angle and residual dipolar coupling constraints (Table 1) were applied in a simulated annealing protocol using the NIH version [61] of XPLOR [62] software. Fifty-nine residual dipolar coupling values measured at 298 K and having values between − 47 Hz and + 37 Hz, and 61 residual dipolar coupling values measured at 283 K and having values between − 52 Hz and + 38 Hz, were used in the final stages of structure refinement. Parameters of the alignment tensor and orientation of the molecule were optimized during the simulated annealing for each conformer in the NMR family using the NIH XPLOR software package. During several iterative cycles of the structure calculations, all experimental restraints were checked and adjusted when necessary using the program NMREST, written-in-house. The database values of conformational torsion angle pseudopotentials [63] were utilized during the calculations. The 20 ps high-temperature dynamics at 1500 K were followed by a cooling phase of 1000 steps of 0.2 ps to 10 K. The values for the final force constants were as follows: NOE restraints, 200 kcal·mol^{-1}·Å^{-2}; dihedral angle restraints, 200 kcal· mol^{-1}·rad^{-2}; residual dipolar couplings, 50 kcal·mol^{-1}·Hz^{-2}; scale factor for conformational database restraints [63], 10. The best 25 out of 50 calculated structures (Fig. 2A) were selected using the criteria of lowest energy of experimental restraints, and analyzed with AQUA and PROCHEK-NMR software [64]. Structure visualization and analysis were carried out using the INSIGHTII software package (Accelrys Software Inc., San Diego, CA, USA) and MOLMOL [65].

NMR dynamics analysis

The R_1 values were deduced from the data acquired as a pseudo-3D experiment with the relaxation delays 8.6 ms, 24.7 ms, 48.6 ms, 96.9 ms, 193.2 ms, 345.7 ms, 498.2 ms, 594.5 ms, 795.2 ms, 1196.4 ms and 1597.7 ms, and the R_2 values were derived from data with relaxation delays of 8.5 ms, 17.1 ms, 25.6 ms, 34.1 ms, 42.6 ms, 51.2 ms, 59.7 ms, 68.2 ms, 76.7 ms, 93.8 ms and 119.4 ms. A 4 s ^{1}H

saturation was applied as a relaxation delay for NOE enhancement in the heteronuclear NOE experiment. Values of R_1 and R_2 with their SDs were obtained from nonlinear fitting of the integrated peak volumes, measured using the nlinLS procedure from the NMRPIPE package [49]. SDs of the ^{15}N,^{1}H-NOE values were calculated using the rms noise of the background regions [66], and were further checked and corrected using two independently collected experimental datasets.

The overall correlation time was calculated from the R_2/R_1 ratios [55]. The calculations yield an average overall correlation time value of 20.2 ± 0.8 ns at 278 K and of 11.5 ± 0.5 ns at 298 K. The overall correlation time was treated as a fixed parameter in subsequent analysis of the relaxation data.

Experimental values of the relaxation parameters were interpreted using the model-free formalism [67] with extensions to include slower internal motions [37] and chemical exchange contributions R_{ex} to the transverse relaxation rates [68] under the assumptions of both isotropic and axially symmetric anisotropic rotational diffusion. Several motional models that included combinations of optimized internal motion parameters S^2 (order parameter), τ_e (effective correlation time of internal motion) and R_{ex} (chemical exchange contribution to the transverse relaxation rate) were used. All calculations were carried out using the program RELAXFIT, written-in-house [69].

The magnitude and orientation of an axially symmetric rotational diffusion tensor were initially estimated by fitting it to the R_2/R_1 ratios for the protein core residues, and further verified by graphical comparison of the experimentally measured parameters against simulated datasets (Fig. 4). Data indicated by gray squares were simulated using the extended Lipari and Szabo [37] and axially symmetric diffusion models, with the following parameters randomly generated (1000 datasets) using the Gauss distribution: average rotational correlation time τ_c 20.8 ± 0.8 ns; ratio of the principal axis of the axially symmetric diffusion tensor ($D_\parallel/D_\perp$) 1.8 ± 0.1; order parameter S^2 within 0.8 ± 0.2; correlation time of fast motion 20 ± 5 ps; correlation time of slow motion τ_s 1 ± 0.1 ns; order parameter of fast motions S_f^2 0.95 ± 0.05. During the calculations, the chemical exchange contribution R_{ex} was set to 0, and all the possible orientations of the vector of the amide NH bond relative to the principal axis of the diffusion tensor (θ angle) were generated. Comparison of the synthetic data with experimentally measured parameters (black circles) shows good correlation. The slope of the simulated data trace on the plot R_2/R_1 against NOE is very sensitive to motional correlation times, particularly to the correlation time of the slow motion τ_s. The range of the dataset on the NOE axis is very sensitive to the value of order parameters; the width of data distribution along the R_2/R_1 axis is specific to the ratio $D_\parallel/D_\perp$.

The obtained parameters τ_s and $D_\parallel/D_\perp$ were then used in the fitting of residue-specific relaxation data. Uncertainties

in the calculated parameters S^2, R_{ex} and internal motion correlation times) were obtained using 500 cycles of Monte-Carlo simulations [70].

Databank accession numbers

The ^{1}H, ^{15}N and ^{13}C chemical shifts have been deposited in the BioMagResBank database (http://www.bmrb.wisc.edu) under the accession number BMRB-6763. The structural data and experimental restraints used in calculations have been submitted to the Protein Data Bank with accession number 2HST.

Acknowledgements

References

1 Alkalaeva EZ, Pisarev AV, Frolova LY, Kisselev LL & Pestova TV (2006) *In vitro* reconstitution of eukaryotic translation reveals cooperativity between release factors eRF1 and eRF3. *Cell* **125**, 1125–1136.

2 Kisselev L, Ehrenberg M & Frolova L (2003) Termination of translation: interplay of mRNA, rRNAs and release factors? *EMBO J* **22**, 175–182.

3 Song H, Mugnier P, Das AK, Webb HM, Evans DR, Tuite MF, Hemmings BA & Barford D (2000) The crystal structure of human eukaryotic release factor eRF1 – mechanism of stop codon recognition and peptidyl-tRNA hydrolysis. *Cell* **100**, 311–321.

4 Kononenko AV, Dembo KA, Kisselev LL & Volkov VV (2004) Molecular morphology of eukaryotic class I translation termination factor eRF1 in solution. *Mol Biol (Mosk)* **38**, 303–311.

5 Bertram G, Bell HA, Ritchie DW, Fullerton G & Stansfield I (2000) Terminating eukaryote translation: domain 1 of release factor eRF1 functions in stop codon recognition. *RNA* **6**, 1236–1247.

6 Frolova L, Seit-Nebi A & Kisselev L (2002) Highly conserved NIKS tetrapeptide is functionally essential in

eukaryotic translation termination factor eRF1. *RNA* **8**, 129–136.

7 Ito K, Frolova L, Seit-Nebi A, Karamyshev A, Kisselev L & Nakamura Y (2002) Omnipotent decoding potential resides in eukaryotic translation termination factor eRF1 of variant-code organisms and is modulated by the interactions of amino acid sequences within domain 1. *Proc Natl Acad Sci USA* **99**, 8494–8499.

8 Seit-Nebi A, Frolova L & Kisselev L (2002) Conversion of omnipotent translation termination factor eRF1 into ciliate-like UGA-only unipotent eRF1. *EMBO Rep* **3**, 881–886.

9 Inagaki Y, Blouin C, Doolittle WF & Roger AJ (2002) Convergence and constraint in eukaryotic release factor 1 (eRF1) domain 1: the evolution of stop codon specificity. *Nucleic Acids Res* **30**, 532–544.

10 Chavatte L, Seit-Nebi A, Dubovaya V & Favre A (2002) The invariant uridine of stop codons contacts the conserved NIKSR loop of human eRF1 in the ribosome. *EMBO J* **21**, 5302–5311.

11 Kolosov P, Frolova L, Seit-Nebi A, Dubovaya V, Kononenko A, Oparina N, Justesen J, Efimov A & Kisselev L (2005) Invariant amino acids essential for decoding function of polypeptide release factor eRF1. *Nucleic Acids Res* **33**, 6418–6425.

12 Liang H & Landweber LF (2005) Molecular mimicry: quantitative methods to study structural similarity between protein and RNA. *RNA* **11**, 1167–1172.

13 Kim OT, Yura K, Go N & Harumoto T (2005) Newly sequenced eRF1s from ciliates: the diversity of stop codon usage and the molecular surfaces that are important for stop codon interactions. *Gene* **346**, 277–286.

14 Salas-Marco J, Fan-Minogue H, Kallmeyer AK, Klobutcher LA, Farabaugh PJ & Bedwell DM (2006) Distinct paths to stop codon reassignment by the variant-code organisms Tetrahymena and Euplotes. *Mol Cell Biol* **26**, 438–447.

15 Ito K, Ebihara K & Nakamura Y (1998) The stretch of C-terminal acidic amino acids of translational release factor eRF1 is a primary binding site for eRF3 of fission yeast. *RNA* **4**, 958–972.

16 Ebihara K & Nakamura Y (1999) C-terminal interaction of translational release factors eRF1 and eRF3 of fission yeast: G-domain uncoupled binding and the role of conserved amino acids. *RNA* **5**, 739–750.

17 Merkulova TI, Frolova LY, Lazar M, Camonis J & Kisselev LL (1999) C-terminal domains of human translation termination factors eRF1 and eRF3 mediate their in vivo interaction. *FEBS Lett* **443**, 41–47.

18 Eurwilaichitr L, Graves FM, Stansfield I & Tuite MF (1999) The C-terminus of eRF1 defines a functionally important domain for translation termination in *Saccharomyces cerevisiae*. *Mol Microbiol* **32**, 485–496.

19 Frolova LY, Merkulova TI & Kisselev LL (2000) Translation termination in eukaryotes: polypeptide

release factor eRF1 is composed of functionally and structurally distinct domains. *RNA* **6**, 381–390.

20 Frolova LY, Tsivkovskii RY, Sivolobova GF, Oparina NY, Serpinsky OI, Blinov VM, Tatkov SI & Kisselev LL (1999) Mutations in the highly conserved GGQ motif of class 1 polypeptide release factors abolish ability of human eRF1 to trigger peptidyl-tRNA hydrolysis. *RNA* **5**, 1014–1020.

21 Nakamura Y & Ito K (2003) Making sense of mimic in translation termination. *Trends Biochem Sci* **28**, 99–105.

22 Poole ES, Askarian-Amiri ME, Major LL, McCaughan KK, Scarlett DJ, Wilson DN & Tate WP (2003) Molecular mimicry in the decoding of translational stop signals. *Prog Nucleic Acid Res Mol Biol* **74**, 83–121.

23 Klaholz BP, Pape T, Zavialov AV, Myasnikov AG, Orlova EV, Vestergaard B, Ehrenberg M & van Heel M (2003) Structure of the *Escherichia coli* ribosomal termination complex with release factor 2. *Nature* **421**, 90–94.

24 Rawat UB, Zavialov AV, Sengupta J, Valle M, Grassucci RA, Linde J, Vestergaard B, Ehrenberg M & Frank J (2003) A cryo-electron microscopic study of ribosome-bound termination factor RF2. *Nature* **421**, 87–90.

25 Petry S, Brodersen DE, Murphy FVT, Dunham CM, Selmer M, Tarry MJ, Kelley AC & Ramakrishnan V (2005) Crystal structures of the ribosome in complex with release factors RF1 and RF2 bound to a cognate stop codon. *Cell* **123**, 1255–1266.

26 Scarlett DJ, McCaughan KK, Wilson DN & Tate WP (2003) Mapping functionally important motifs SPF and GGQ of the decoding release factor RF2 to the Escherichia coli ribosome by hydroxyl radical footprinting. Implications for macromolecular mimicry and structural changes in RF2. *J Biol Chem* **278**, 15095–15104.

27 Chavatte L, Frolova L, Laugaa P, Kisselev L & Favre A (2003) Stop codons and UGG promote efficient binding of the polypeptide release factor eRF1 to the ribosomal A site. *J Mol Biol* **331**, 745–758.

28 Ma B & Nussinov R (2004) Release factors eRF1 and RF2: a universal mechanism controls the large conformational changes. *J Biol Chem* **279**, 53875–53885.

29 Nissen P, Kjeldgaard M & Nyborg J (2000) Macromolecular mimicry. *EMBO J* **19**, 489–495.

30 Seit-Nebi A, Frolova L, Justesen J & Kisselev L (2001) Class-1 translation termination factors: invariant GGQ minidomain is essential for release activity and ribosome binding but not for stop codon recognition. *Nucleic Acids Res* **29**, 3982–3987.

31 Zavialov AV, Mora L, Buckingham RH & Ehrenberg M (2002) Release of peptide promoted by the GGQ motif of class 1 release factors regulates the GTPase activity of RF3. *Mol Cell* **10**, 789–798.

32 Mora L, Heurgue-Hamard V, Champ S, Ehrenberg M, Kisselev LL & Buckingham RH (2003) The essential

role of the invariant GGQ motif in the function and stability in vivo of bacterial release factors RF1 and RF2. *Mol Microbiol* **47**, 267–275.

33 Dubovaia VI, Kolosov PM, Alkalaeva EZ, Frolova L & Kiselev LL (2006) Influence of individual domains of the translation termination factor eRF1 on induction of the GTPase activity of the translation termination factor eRF3. *Mol Biol (Mosk)* **40**, 310–316.

34 Hamelberg D & McCammon JA (2005) Fast peptidyl cis-trans isomerization within the flexible Gly-rich flaps of HIV-1 protease. *J Am Chem Soc* **127**, 13778–13779.

35 Gao F, Mer G, Tonelli M, Hansen SB, Burghardt TP, Taylor P & Sine SM (2006) Solution NMR of acetylcholine binding protein reveals agonist-mediated conformational change of the C-loop. *Mol Pharmacol* **70**, 1230–1235.

36 Kleerekoper Q, Hecht JT & Putkey JA (2002) Disease-causing mutations in cartilage oligomeric matrix protein cause an unstructured Ca^{2+} binding domain. *J Biol Chem* **277**, 10581–10589.

37 Clore GM, Szabo A, Bax A, Kay LE, Driscoll PC & Gronenborn AM (1990) Deviations from the simple 2-parameter model-free approach to the interpretation of N-15 nuclear magnetic-relaxation of proteins. *J Am Chem Soc* **112**, 4989–4991.

38 Ban N, Nissen P, Hansen J, Moore PB & Steitz TA (2000) The complete atomic structure of the large ribosomal subunit at 2.4 A resolution. *Science* **289**, 905–920.

39 Yusupov MM, Yusupova GZ, Baucom A, Lieberman K, Earnest TN, Cate JH & Noller HF (2001) Crystal structure of the ribosome at 5.5 Å resolution. *Science* **292**, 883–896.

40 Cannone JJ, Subramanian S, Schnare MN, Collett JR, Du D'Souza LMY, Feng B, Lin N, Madabusi LV, Muller KM, Pande N *et al.* (2002) The comparative RNA web (CRW) site: an online database of comparative sequence and structure information for ribosomal, intron, and other RNAs. *BMC Bioinformatics* **3**, 2.

41 Jeffrey GA (1997) *An Introduction to Hydrogen Bonding*. Oxford University Press, New York, NY.

42 Molday RS, Englande. SW & Kallen RG (1972) Primary structure effects on peptide group hydrogen-exchange. *Biochemistry* **11**, 150–158.

43 Dincbas-Renqvist V, Engstrom A, Mora L, Heurgue-Hamard V, Buckingham R & Ehrenberg M (2000) A post-translational modification in the GGQ motif of RF2 from Escherichia coli stimulates termination of translation. *EMBO J* **19**, 6900–6907.

44 Heurgue-Hamard V, Champ S, Mora L, Merkulova-Rainon T, Kisselev LL & Buckingham RH (2005) The glutamine residue of the conserved GGQ motif in Saccharomyces cerevisiae release factor eRF1 is methylated by the product of the YDR140w gene. *J Biol Chem* **280**, 2439–2445.

45 Seit Nebi A, Frolova L, Ivanova N, Poltaraus A & Kisselev L (2000) Mutation of a glutamine residue in the universal tripeptide GGQ in human eRF1 termination factor does not cause complete loss of its activity. *Mol Biol (Mosk)* **34**, 899–900.

46 Williamson RA, Muskett FW, Howard MJ, Freedman RB & Carr MD (1999) The effect of matrix metalloproteinase complex formation on the conformational mobility of tissue inhibitor of metalloproteinases-2 (TIMP-2). *J Biol Chem* **274**, 37226–37232.

47 Privalov PL, Jelesarov I, Read CM, Dragan AI & Crane-Robinson C (1999) The energetics of HMG box interactions with DNA: thermodynamics of the DNA binding of the HMG box from mouse Sox-5. *J Mol Biol* **294**, 997–1013.

48 Baleja JD, Marmorstein R, Harrison SC & Wagner G (1992) Solution structure of the DNA-binding domain of Cd2-Gal4 from *Saccharomyces cerevisiae*. *Nature* **356**, 450–453.

49 Delaglio F, Grzesiek S, Vuister GW, Zhu G, Pfeifer J & Bax A (1995) NMRPipe: a multidimensional spectral processing system based on UNIX pipes. *J Biomol NMR* **6**, 277–293.

50 Zimmerman DE, Kulikowski CA, Huang Y, Feng W, Tashiro M, Shimotakahara S, Chien C, Powers R & Montelione GT (1997) Automated analysis of protein NMR assignments using methods from artificial intelligence. *J Mol Biol* **269**, 592–610.

51 Ivanova EV, Kolosov PM, Birdsall B, Kisselev LL & Polshakov VI (2006) NMR assignments of the middle domain of human polypeptide release factor eRF1. *J Biomol NMR* **36**, suppl. 1, 8.

52 Bax A & Grzesiek S (1993) Methodological advances in protein NMR. *Acc Chem Res* **26**, 131–138.

53 Ruckert M & Otting G (2000) Alignment of biological macromolecules in novel nonionic liquid crystalline media for NMR experiments. *J Am Chem Soc* **122**, 7793–7797.

54 Ottiger M, Delaglio F & Bax A (1998) Measurement of J and dipolar couplings from simplified two-dimensional NMR spectra. *J Magn Reson* **131**, 373–378.

55 Kay LE, Torchia DA & Bax A (1989) Backbone dynamics of proteins as studied by ^{15}N inverse detected heteronuclear NMR spectroscopy: application to staphylococcal nuclease. *Biochemistry* **28**, 8972–8979.

56 Boyd J, Hommel U & Campbell ID (1990) Influence of cross-correlation between dipolar and anisotropic chemical-shift relaxation mechanisms upon longitudinal relaxation rates of N-15 in macromolecules. *Chem Phys Lett* **175**, 477–482.

57 Cornilescu G, Delaglio F & Bax A (1999) Protein backbone angle restraints from searching a database for chemical shift and sequence homology. *J Biomol NMR* **13**, 289–302.

58 Polshakov VI, Frenkiel TA, Birdsall B, Soteriou A & Feeney J (1995) Determination of stereospecific assignments, torsion-angle constraints, and rotamer populations in proteins using the program AngleSearch. *J Magn Reson B* **108**, 31–43.

59 Nilges M, Macias MJ, O'Donoghue SI & Oschkinat H (1997) Automated NOESY interpretation with ambiguous distance restraints: the refined NMR solution structure of the pleckstrin homology domain from beta-spectrin. *J Mol Biol* **269**, 408–422.

60 Linge JP, Habeck M, Rieping W & Nilges M (2003) ARIA: automated NOE assignment and NMR structure calculation. *Bioinformatics* **19**, 315–316.

61 Schwieters CD, Kuszewski JJ, Tjandra N & Clore GM (2003) The Xplor-NIH NMR molecular structure determination package. *J Magn Reson* **160**, 65–73.

62 Brünger AT (1992) *X-PLOR: a System for X-Ray Crystallography and NMR*, 17th edn. Yale University Press, New Haven, CT.

63 Kuszewski J, Gronenborn AM & Clore GM (1997) Improvements and extensions in the conformational database potential for the refinement of NMR and X-ray structures of proteins and nucleic acids. *J Magn Reson* **125**, 171–177.

64 Laskowski RA, Rullmann JA, MacArthur MW, Kaptein R & Thornton JM (1996) AQUA and PROCHECK-NMR: programs for checking the quality of protein structures solved by NMR. *J Biomol NMR* **8**, 477–486.

65 Koradi R, Billeter M & Wuthrich K (1996) MOLMOL: a program for display and analysis of macromolecular structures. *J Mol Graph* **14**, 51–55.

66 Farrow NA, Muhandiram R, Singer AU, Pascal SM, Kay CM, Gish G, Shoelson SE, Pawson T, Forman-Kay JD & Kay LE (1994) Backbone dynamics of a free and phosphopeptide-complexed Src homology 2 domain studied by ^{15}N NMR relaxation. *Biochemistry* **33**, 5984–6003.

67 Lipari G & Szabo A (1982) Model-free approach to the interpretation of nuclear magnetic-resonance relaxation in macromolecules. 2. Analysis of experimental results. *J Am Chem Soc* **104**, 4559–4570.

68 Clore GM, Driscoll PC, Wingfield PT & Gronenborn AM (1990) Analysis of the backbone dynamics of interleukin-1 beta using two-dimensional inverse detected heteronuclear 15N–1H NMR spectroscopy. *Biochemistry* **29**, 7387–7401.

69 Polshakov VI, Birdsall B, Frenkiel TA, Gargaro AR & Feeney J (1999) Structure and dynamics in solution of the complex of *Lactobacillus casei* dihydrofolate reductase with the new lipophilic antifolate drug trimetrexate. *Protein Sci* **8**, 467–481.

70 Tillett ML, Blackledge MJ, Derrick JP, Lian LY & Norwood TJ (2000) Overall rotational diffusion and internal mobility in domain II of protein G from *Streptococcus* determined from N-15 relaxation data. *Protein Sci* **9**, 1210–1216.

71 Altschul SF, Madden TL, Schaffer AA, Zhang J, Zhang Z, Miller W & Lipman DJ (1997) Gapped BLAST and PSI-BLAST: a new generation of protein database search programs. *Nucleic Acids Res* **25**, 3389–3402.

Supplementary material

The following supplementary material is available online:

Fig. S1. Plot of the number and distribution of NOEs against the amino acid sequence used in structure calculation of the M domain of human eRF1.

Fig. S2. The Ramachandran map plot (ϕ and ψ torsion angles for the protein backbone) of all 25 conformers of the NMR family of solution structures of the M domain of human eRF1.

Fig. S3. A surface representation of the M domain of human eRF1, mapping the electrostatic potential.

Fig. S4. A comparison of part of the protein backbone structure of the representative solution structure of the human eRF1 M domain and the Ca trace in the crystal structure of RF1 in the whole ribosome structure (Protein Data Bank code 2b64) presented as a stereo view.

This material is available as part of the online article from http://www.blackwell-synergy.com

Please note: Blackwell Publishing is not responsible for the content or functionality of any supplementary materials supplied by the authors. Any queries (other than missing material) should be directed to the corresponding author for the article.